minerals

MDPI

Article

Recovery of Rare Earth Elements from Ion-Adsorption Deposits Using Electrokinetic Technology: The Soil Conductivity Mechanism Study

Shichang Kang [1,2,3], Bowen Ling [4,5], Xiaoliang Liang [1,2,3], Gaofeng Wang [1,2,3,*], Jie Xu [1,2,3], Yongjin Xu [1,2,3], Runliang Zhu [1,2,3], Jingming Wei [1,2,3], Jianxi Zhu [1,2,3] and Hongping He [1,2,3]

1   CAS Key Laboratory of Mineralogy and Metallogeny/Guangdong Provincial Key Laboratory of Mineral Physics and Material, Guangzhou Institute of Geochemistry, Chinese Academy of Sciences, Guangzhou 510640, China; kangshichang@gig.ac.cn (S.K.); liangxl@gig.ac.cn (X.L.); xujie777@gig.ac.cn (J.X.); xuyongjin@gig.ac.cn (Y.X.); zhurl@gig.ac.cn (R.Z.); weijm@gig.ac.cn (J.W.); zhujx@gig.ac.cn (J.Z.); hehp@gig.ac.cn (H.H.)
2   CAS Center for Excellence in Deep Earth Science, Guangzhou 510640, China
3   University of Chinese Academy of Sciences, Beijing 100049, China
4   Institute of Mechanics, Chinese Academy of Sciences, Beijing 100190, China; lingbowen@imech.ac.cn
5   School of Engineering Science, University of Chinese Academy of Sciences, Beijing 100049, China
*   Correspondence: wanggaofeng@gig.ac.cn

Abstract: Rare earth elements (REEs) are essential raw materials for modern industries but mining them has caused severe environmental issues, particularly the recovery of heavy REEs (HREEs) from ion-adsorption deposits (IADs). Very recently, an emerging technology, electrokinetic mining (EKM), has been proposed for the green and efficient recovery of REEs from IADs. However, the conduction mechanism of the weathering crust soil, which is also a prerequisite for EKM, remains unclear, making the EKM process unpredictable. Here, we systematically investigated the conductivity of weathering crust soil in the presence of light REEs (LREEs, i.e., La^{3+} and Sm^{3+}) and HREEs (Er^{3+} and Y^{3+}), respectively. Results suggested that the voltage was dynamically and spatially redistributed by the movement of REEs and water during EKM, and the conventional assumption of the linear distribution of voltage leads to an inaccurate description of soil voltage. We proposed an improved Archie's equation by coupling the mechanisms of liquid phase and solid-liquid interface conduction, which can predict soil conductivity more precisely. Moreover, the extended Archie's equation is able to recalculate the voltage distribution at distinct times and spaces well during EKM. More importantly, the water content in field-scale weathered-crust soils can be retrieved by the newly proposed Archie's equation, which helps optimize the leaching wells and improve the recovery rate of REE. This study focuses on the conduction mechanism of weathering crust soil, which provides a theoretical basis for better use of the EKM technology and promotes mining efficiency fundamentally.

Keywords: electrokinetic mining; rare earth elements; recovery; soil conductivity; Archie's equation

1. Introduction

Rare earth elements (REEs), valued for their exceptional physical and chemical properties, find wide applications in modern industries including electronics, metallurgy, clean energy, and high-tech manufacturing [1,2]. Of particular significance are the heavy REEs (HREEs), which possess unparalleled value as they are irreplaceable on rockets, satellites, aircraft carriers, and fighters. Ion-adsorption deposits (IADs) of REEs are the main source of HREEs and provide more than 90% production [3,4], where REEs are absorbed onto clay minerals in the weathering crust soil of the IADs ore as ions or hydrated ions [5,6]. The adsorbed REEs can be desorbed and transported by adding leaching agents (e.g., highly concentrated electrolyte solutions). The mining of IADs is predominantly based on leaching techniques.

Currently, the commonly used leaching agent is ammonium salt [7,8]. In the leaching process, a large amount of ammonium salts (7–10 t $(NH_4)_2SO_4$ for 1 t REE oxide production) is injected into the soil to achieve a high recovery rate of REE, which has resulted in severe ammonia nitrogen contaminations of water and soil, and the release of unexpected metals [9]. In addition, the leaching technique has a low recovery rate of 40%–60% due to the leakage of REE fluids into pores of the weathering crust soil [10]. Various methods have been proposed to address these issues [11,12]. Among these, the electrokinetic mining (EKM) technique [13,14] is an emerging approach with mining potentials to reduce the environmental impact and improve the recovery rate (>90%). The core of EKM applies an electric field to drive and control ion migration unidirectionally, coupled with gravity, pressure, and concentration to promote the infiltration of leaching agents in soil [15]. Though EKM has advantages including low environmental pollution and economic cost [16,17], the technology is still in its early stages. Many significant working mechanisms, particularly the soil conductivity mechanism that is regarded as the prerequisite of EKM technology, have not been well understood. This leads to difficulties in predicting and controlling the actual extraction behavior, designing and optimizing the EKM parameters, and setting and implementing the EKM process. Therefore, it is urgent to clarify the soil conductivity mechanism and accurately obtain voltage distribution information in soils to guide the EKM process for recovering REEs.

In previous studies, the conductivity was thought to be uniformly distributed in the soil. Accordingly, the effective electric field theory is proposed based on a linear model of voltage is proposed [18]. However, because ions and water are mobilized during the electrokinetic process, the soil conductivity changes dynamically. Unfortunately, such a phenomenon has not been recognized, resulting in inaccurate predictions by using the linear model. In IADs, the soils are a complicated three-phase system of solid, liquid, and gas, which leads to the complexity of the soil conduction mechanism [19,20]. In the natural state, the soil is unsaturated, where liquid water is separated by soil particles and air, resulting in poor electrical conductivity [21]. During the EKM process, a steady stream of leaching agents is injected into the ore body, and the air in the soil is gradually expelled, creating a saturated state of the soil and increasing the soil's conductivity [22]. In a previous study, it was suggested the electrical conductivity increased from 0 to 2000 μs cm^{-1} due to the increase in soil humidity from 25% to 47% [23]. Furthermore, there is a linear or quadratic relationship between conductivity and moisture content of the soil [24]. Pure water itself is not a good conductor and the conductivity of a solution results mainly from soluble ions [25]. Therefore, the ions in soil play a significant role in conducting electricity. For an ion, the concentration and charge play important roles in the conductivity. In dilute solutions, the conductivity is proportional to the concentration and charge [26]. Therefore, the ion content may be determined from the conductivity of the soil. As such, the migration path of an ion in soil can be tracked by measuring the conductivity of the soil at various locations.

However, there are two conduction paths including solid-liquid interface and liquid phase conductivity in the soil system, which make the interpretation between the ion content and conductivity challenging [27,28]. In IADs, REEs are mainly enriched on the surface of clay minerals in the form of ions or hydrated ions [29]. Generally, the conductivity of the carrier, i.e., clay mineral, is poor and can be ignored [30]. However, during the EKM process, REEs on the surface of clay minerals are activated and migrated, and the conductivity of the solid-liquid interface cannot be ignored [31]. In addition, the carrier mineral has defects and its surface is conductive by electrical double layers [32,33], which makes the traditional Archie's equation unable to effectively describe the electrical conductivity of soil in the EKM process. This further increases the difficulty of interpreting the conductivity mechanism of the weathering crust soil [34,35]. Therefore, distinguishing the influence of the solid-liquid interface and liquid phase on the conductivity of the soil in IADs is a top priority.

In this study, we developed an extended Archie's equation by coupling the mechanisms of solid-liquid interface and liquid phase conductivity. The conductivity of the

weathering crust soil was investigated with the existence of LREEs (La^{3+} or Sm^{3+}) or HREEs (Er^{3+} or Y^{3+}), respectively. The relationship between the conductivity and ion concentration, charge, and moisture has been determined. The newly improved Archie's equation was applied to predict the conductivity of weathering crust soil during the EKM process, which achieved results consistent with the experimental data. Moreover, we used the improved Archie's equation to recalculate the voltage distribution of the weathering crust soil during EKM. Significantly, we also successfully predicted the water content of the weathering crust soil in the field with the extended Archie's equation, which will help optimize the leaching wells and improve the recovery rate of REE.

2. Materials and Methods

2.1. Materials

The weathering crust soil was collected from MaoFeng Moutain in Guangzhou City, Guangdong Province, China. The sample was separated by the quartering method. The water content of the soil was 4.49%. Lanthanum, samarium, erbium, and yttrium nitrate hexahydrates in analytical reagent were manufactured by Shanghai Aladdin Biochemical Technology Co., Ltd. (Shanghai, China). Potassium chloride and ammonium sulfate in analytical reagent were purchased from Sinopharm Chemical Reagent Co., Ltd. (Shanghai, China). A 1000 ppm stock solution of each REE was prepared by dissolving the powder reagents.

2.2. The Simulated EKM Experiments

To investigate variations of soil conductivity during the EKM and verify the extended Archie's equation, simulated EKM experiments were conducted in a length of 50 cm column as shown in Figure 1. First, the soil was sandwiched with geotextile and graphite electrode. Then, the simulated experiments are mainly conducted in two steps. Initially, 1000.0 g of soil was wetted with 200.0 g of water for 12 h to simulate the hydrated weathering crust soil. Subsequently, the anode was continuously injected with 200 and 400 ppm of La^{3+}, Sm^{3+}, Er^{3+}, and Y^{3+} solution via a Markov bottle, respectively, after which a voltage of 50 V was exerted between the anode and the cathode for simulating EKM process. During the simulated EKM process, the voltages were monitored three times by a voltmeter (DELIXI 860d, Delixi Electric Co., Ltd., Leqing, China) at positions of 1.5 (P1), 16.5 (P2), 31.5 (P3), and 46.5 cm (P4) away from anode, respectively, and three sections (S1, S2, and S3 named from anode to cathode) were constructed by these four positions as Figure 1 shown. Meanwhile, the current was recorded on an amperemeter (CY-high precision, Chiyi Hardware, Huaian, China). The water contents in P1–P4 were measured at various EKM time intervals (i.e., 1, 3, 6, 12, 24, 36, 48, 60, 72, 84, 96, and 120 h) as well. The concentrations of REE in P1–P4 were analyzed every 24 h by an inductively coupled plasma optical emission spectrometer (ICP-OES, OPTIMA 2000DV, PerkinElmer, Waltham, MA, USA). The collected soil samples were sufficiently exchanged with 0.2 M ammonium sulfate for 24 h to extract the ion-exchangeable REE.
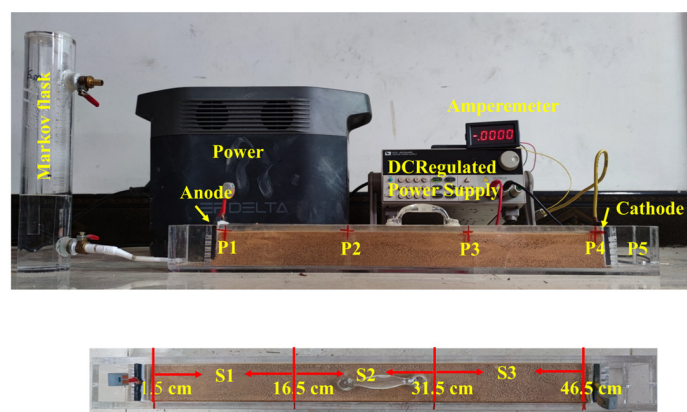
Figure 1. Schematic diagrams of experimental apparatus and sampling locations.

2.3. Measurement of the Solution Conductivity

The conductivity of the solution is measured by a multi-parameter meter (HQ 40 d, Hach Co., Ltd., Ames, IA, USA). Before the test, different concentrations of potassium chloride (KCl) solutions were used to calibrate the instrument. The probe was immersed three times in a plastic bottle containing 250 mL of REE solution with various concentrations (i.e., 0.1, 0.5, 1.0, 5.0, 10.0, 50.0, 100.0, 200.0, 300.0, 400.0, 500.0, and 1000.0 ppm) to detect the conductivity of the solution. In general, the conductivity of a strong electrolyte is proportional to its concentration and Equation (1) is applied to describe its conductivity [36].

$$\sigma = K \times z \times c + \sigma_0 \tag{1}$$

where σ is the conductivity ($\Omega^{-1}\ m^{-1}$), K is the conductivity per unit concentration ($\Omega^{-1}\ m^{-1}\ L\ mg^{-1}$), z is the charge of the ion and it is 3 for REEs in this study, c is the concentration of the solution ($mg\ L^{-1}$), and σ_0 is the conductivity of the pure water ($\Omega^{-1}\ m^{-1}$). The parameters obtained from Equation (1) were statistically significant at a 95% confidence level.

2.4. Measurement of the Soil Conductivity

To build the relationship between the soil conductivity and REE concentration, soils with various concentrations of REE solutions were prepared. The weathering soil, weighing 350 g, was immersed in a solution containing La^{3+}, Sm^{3+}, Er^{3+}, and Y^{3+} ions at concentrations of 100 mg L^{-1} (low concentration, L), 300 mg L^{-1} (middle concentration, M), and 500 mg L^{-1} (high concentration, H), respectively, for 36 h. Afterward, the mixture was washed with 3 L of water and dried at 105 °C to achieve REE-L, REE-M, and REE-H types of the simulated weathering crust soil, respectively. For comparison, the weathering crust soil was also treated with deionized water, and the sample was marked as 'Origin'. The water-soluble REE in REE-L, REE-M, and REE-H was extracted by adding 1.00 g of soil into 10 mL of water for 24 h of agitation. After a complete washing, the supernatant was obtained by centrifugation at $1199\times g$ (TGL 18 M, Lu Xiangyi Centrifuge Instrument Co., Ltd., Shanghai, China) and measured by an ICP-OES to determine the water-soluble REE concentration (c_{aq}). The sediment was further used to extract the ion-exchangeable REE (c_s) by adding 10 mL of $(NH_4)_2SO_4$ solution (0.2 mol L^{-1}). As such, the distribution coefficient can be expressed as Equation (2) [37].

$$K_d = \frac{c_s}{c_{aq}} \tag{2}$$

where K_d is the distribution coefficient of concentration in liquid and solid. The conductivity of the soil was detected using the four-electrode resistance method which was conducted in a length of 10 cm column. During the test, graphite electrodes are placed at both ends of the column. When the specific amount (0.15, 0.25, 0.35, and 0.45) of water is standing and diffusing in the soil for 12 h, the moisture content is corrected by the change of mass. Then, the conductivity of the soil is conversed by a DC-regulated power supply (IT6722, ITECH, Nanjing, China) and a voltmeter. The applied voltage of the graphite electrode was increased from 5 to 75 V, and then the voltage in the middle 5 cm section was measured and the current was recorded by an amperemeter. Finally, the conductivity is converted according to Ohm's law.

2.5. Development of the Extended Archie's Equation for Soil Conductivity

In the EKM process, the weathering crust soil between electrodes could be taken as a resistance element. The conductivity of the weathering crust soil and the voltages at different locations can be calculated by Ohm's law as Equations (3) and (4) shown, respectively.

$$\sigma = \frac{IL}{US} \tag{3}$$

$$\frac{U_1}{U_2} = \frac{\sigma_1}{\sigma_2} \tag{4}$$

where I is the current (A), L is the length of the detected area (m), U is the voltage (V), and S is the cross area (m^2). where U_1 and U_2 are voltages of resistance elements 1 and 2, σ_1 and σ_2 are conductivities of elements 1 and 2, respectively. In 1942, Archie proposed an empirical law that related to conductivity and porosity, and the model was widely used in reservoir engineering and petrophysics [38,39]. Then, Archie's equation, as displayed in Equation (5), has broader applications in unsaturated porous media [40].

$$\sigma_t = k\varphi^m S_r^n \sigma \tag{5}$$

where σ is the conductivity of soil, k is unitless empirical constant, φ is the porosity, m is a shape (cementation) exponent, S_r is the saturation degree and it is described by moisture and porosity (Equation (6)). The saturation exponent n is commonly assumed to have a value of about 2 [41]. σ is the sum of the solid-liquid interface and liquid phase conductivity (Equation (7)).

$$S_r = \frac{\theta_V}{\varphi} = \frac{\rho\theta_w}{\varphi} \tag{6}$$

where θ_V and θ_w are the moisture contents in volume and weight, respectively. ρ is the density.

$$\sigma = \varphi\sigma_w + (1 - \varphi)\sigma_s \tag{7}$$

where σ_s and σ_w are conductivities of solid-liquid and the liquid phase related to the concentration, respectively, in the dilute solution, the conductivity is proportional to the ion concentration and charge as shown in Equation (1). Similarly, we assumed that the soil conductivity is proportional to the total concentrations of various ions in the weathering crust soil, inducing Equations (1) and (5)–(7), the soil conductivity can be expressed as Equation (8) when the parameters were simplified.

$$\sigma_t = k\rho^n \varphi^{m-n}(\varphi\sigma_w + (1-\varphi)\sigma_s) = K_1 \times \theta_w^2 \times \left(\frac{K_2 z c_{aq}}{\theta_w} + K_3 z c_s \right) + K_4 \tag{8}$$

where σ_t (Ω^{-1} m^{-1}) is the total conductivity of the soil, K_1, K_2 (Ω^{-1} m^{-1} L mg^{-1}), K_3 (Ω^{-1} m^{-1} kg mg^{-1}), and K_4 (Ω^{-1} m^{-1}) are the parameters of moisture, liquid, solid, and water, respectively. K_2 and K_4 are calculated from the parameters of Equation (1) and blank pure solution. K_1 and K_3 calculated by Equation (8) were statistically significant at a 95% confidence level. θ_w is the moisture content in weight. c_{aq} (mg L^{-1}) is the concentration in the liquid phase, c_s (mg kg^{-1}) is the concentration in the weathering crust soil.

*2.6. Field-Scale Experiments*

To determine the feasibility of the extended Archie's Equation in predicting the water content of the soil, field-scale experiments as shown in Figure S1a were carried out in Meizhou City, Guangdong Province. The field-scale experiments were operated on a typical IAD with a dimension of 9 × 3 m (Figure S1b). During the test, four electrodes were successively inserted into the soil at a depth of 5 cm at an interval of 1 m in a line, and the ground resistance meter (VC4105A, Bei Cheng (Hong Kong) Technology Co., Ltd., China) was connected for measurement. During the test, the voltage is given by the two edge electrodes (Electrode 1 and 4) and the resistance can be obtained when the voltage is detected by the inner electrodes (Electrode 2 and 3). Then, Ohm's law is applied to converse the conductivity ($\sigma = \frac{1}{\rho_\Omega}$, where ρ_Ω (Ω^{-1} m^{-1}) is the resistivity) and the moisture content was inversed by the extended Archie's Equation (Equation (8)). The test was repeated three times at an interval of 5 min. All tests of resistivity were completed after all electrodes were extended by 1 m to 10 m. In order to verify the moisture, soil obtained in the middle was dried at 105 °C.

3. Results and Discussion

3.1. Redistribution of the Voltage in Weathering Crust Soil during EKM

To clarify the soil conductive characteristic in the EKM process, the simulated EKM experiments were conducted in a 50 cm column and the results are shown in Figure 2. (Figure 2a–d) depicted the variation of the voltage at various positions of the weathering crust soil when 200 ppm of La^{3+}, Sm^{3+}, Er^{3+}, and Y^{3+} solution was injected from the anode, respectively. The result suggested that the voltage was not linearly distributed from the anode to the cathode and changed dynamically with increasing EKM time (Figure 2).
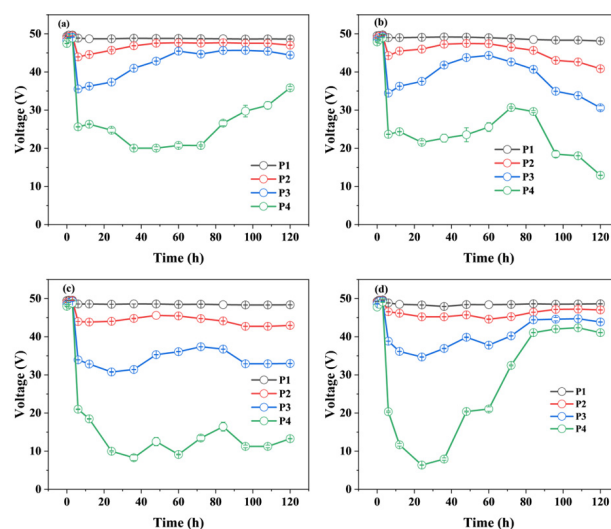
Figure 2. Variations of voltage at P1–P4 positions in the simulated EKM experiment with the injection of 200 ppm of La^{3+} (**a**), Sm^{3+} (**b**), Er^{3+} (**c**), and Y^{3+} (**d**) solution, respectively.

As for four different REEs, the voltage varied differently with time. For the LREE La^{3+} (Figure 2a), the voltages at P1, P2, P3, and P4 are 49.37, 48.87, 48.20, and 47.47 V, respectively, at 0 h due to the unsaturation of geotextile and large surface resistance of cathode. In the first 6 h, voltages at P1–P4 changed little, which may result from the low water content of the weathering crust soil (Figure 3a) and the unsaturation of geotextile, i.e., the electrical path was not connected. At 6 h, the redistribution of voltage occurred the voltage of P1, P2, P3, and P4 reached 48.87, 43.95, 35.54, and 25.62 V, respectively. This phenomenon was caused by the saturation of the La^{3+} solution; the moisture content at P4 reached 42.47% at 6 h (Figure 3a). A total of 11.9 mL solution was also collected in the cathode chamber of the column (Figure 3b). As such, the resistance of the weathering crust soil and geotextile plummeted [42]. Correspondingly, the current density rose sharply from 0.0010 to 0.1317 A m^{-2} at 6 h as shown in Figure 3b. After 6 h, the voltage of weathering crust soil at P1, P2, P3, and P4 varied differently due to the movement of water and ions. The voltage of P1 decreased slightly from 48.87 to 48.63 V as it was soaked with La^{3+} (the concentration of La^{3+} increased as shown in Figure 3c) and H^+ (the pH decreased from 4.08 to 3.82 as shown in Figure 3d), yielding the high conductivity of the weathering soils near the anode. The voltage of P2 increased from 43.95 to 47.67 V from 6 to 60 h and then decreased to 47.03 V at 120 h, which was insured by the movement of La^{3+} (Figure 3c) and H^+ (Figure 3d). Similarly, the voltage of P3 showed the same trend the voltage increased from 35.54 to 45.47 V from 6 to 60 h and decreased to 44.43 V at 120 h. The voltage at P4 decreased to 20.02 V due to the generation of OH^- in the cathode as verified by the neuter cleaner at the P5 position and the increase in pH at the P4 position.

For Sm^{3+}, the distribution of voltage at P1–P4 positions in the first 6 h was similar to that of La^{3+} and the voltage at P1–P4 positions was close to 50 V as shown in Figure 2b, due to the unsaturation of the weathering crust soils (Figures S2a and 4a) and the geotextile. At 6 h, the voltages at P1–P4 positions were also redistributed, which reached 48.99, 44.29, 34.46,

and 23.66 V, respectively. The current density was sharply increased from 0 to 0.1647 A m^{-2} (Figure 4b) due to the connection of the electrical path. After 6 h, the voltage at P1–P3 showed a similar trend as La^{3+}, where the voltage at P1 decreased slightly to 40.85 V, and the voltage at P2 and P3 showed an inverted "V-shape" due to the movement of Sm^{3+} (Figure S2b) and H^{+} (Figure S2c). Unlike La^{3+}, the voltage at P4 increased to 30.67 V at 72 h and decreased to 12.93 V at 120 h. The cathode produces a large number of hydroxides, blocking the current transmission channel, and making the voltage at P4 rise. The pH at P4 and P5 would decrease like that at P1–P3, considering that there was no generated OH^{-}. However, the pH at P5 was maintained at neutral, and the pH at P4 increased at 60 h, as shown in Figure 3d, which was different from that at P1–P3. Results indicate that the generated OH^{-} transports from the cathode to P4. Based on this, we further speculated that a large number of OH^{-} was generated because OH^{-} needed to overcome hydraulic gradients and soil buffering to reach P4.
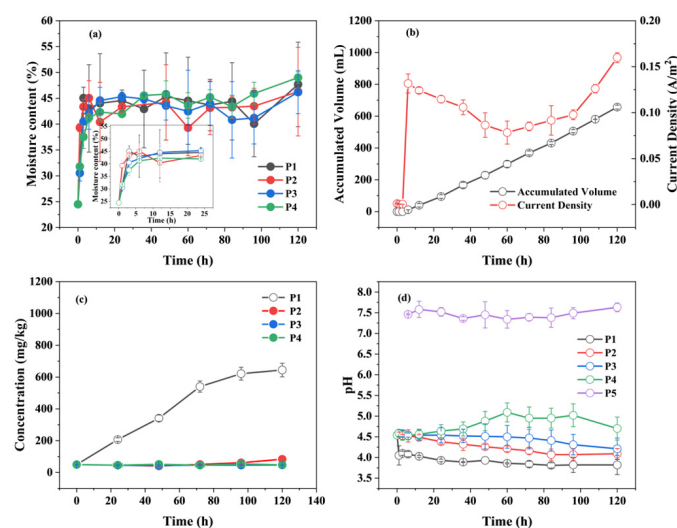
Figure 3. Variations of the moisture content (**a**), accumulative volume and current density (**b**), concentration of La^{3+} (**c**), and pH (**d**), respectively, at distinct positions (P1–P5) in the simulated EKM experiment with the injection of 200 ppm of La^{3+} solution.
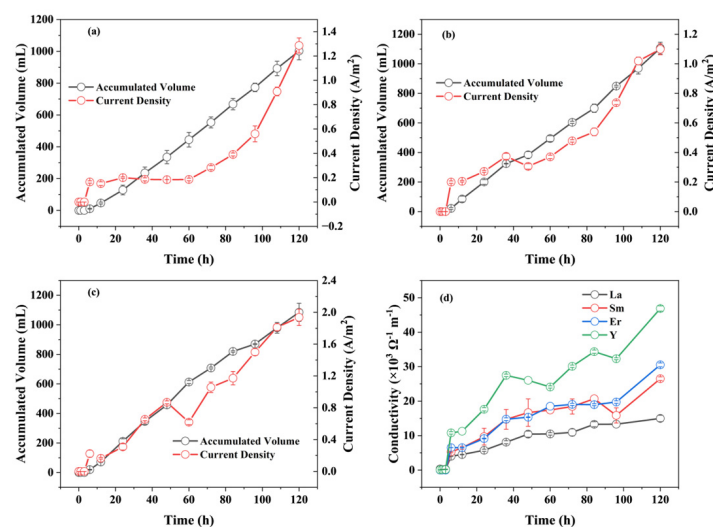
Figure 4. Variations of current density and accumulative volume at P5 in the simulated EKM experiment with the injection of 200 ppm of Sm^{3+} (**a**), Er^{3+} (**b**), and Y^{3+} (**c**) solution. Comparison of the conductivity of the weathering crust soil with the injection of 200 ppm of La^{3+}, Sm^{3+}, Er^{3+}, and Y^{3+}, respectively (**d**).

For the HREE Er^{3+}, in the first 6 h, the voltages at P1–P4 were close to 50 V (Figure 2c). At 6 h, the voltage was redistributed at P1–P4 due to the connection of the electrical path. The moisture content at P1–P4 was gradually saturated (Figure S4a) and 21.1 mL of solution was collected (Figure 4b). Correspondingly, the current density increased sharply. After 6 h, the variation of the voltage at P1–P3 showed the same trend as that of LREEs (La^{3+} and Sm^{3+}) due to the transport of Er^{3+} and H^+. Distinctively, the voltage at P4 fluctuated, which probably resulted from the complex reactions near P4, such as electrolysis, precipitation, and acid-base neutralization reactions. The pH in the P5 solution fluctuated as well.

The voltage variations of another HREE Y^{3+} showed a similar trend to that of LREEs in the first 6 h. However, after 6 h, the voltage at P2 declined to 42.27 V, likely attributed to the accelerated transport of HREEs compared to LREEs, and the voltage at P3 and P4 floated because of the complex reaction like the other HREE, i.e., Er^{3+}. These findings indicate that the voltage fluctuations in the weathering crust soil vary depending on the presence of LREEs and HREEs, reflecting differences in their transport velocities and electric reactions. In Figure S4c, although the pH at P5 was large and the highest reached close to 10, the pH at P4 showed a decreasing trend, which indicated the acid-base reaction occurred in the section between P4 and the cathode.

Generally, the voltage of the weathering crust soil is redistributed in space and time due to the movement of water and ions in the column. According to the definition (σ), the conductivity is related to the current and voltage, as shown in Equation (3):

We applied it to calculate the conductivity of the weathering crust soil at P1 and the results are shown in Figure 4d. As shown in Figure 4d, it is found that the conductivity of REEs increased dynamically due to the concentrations of La^{3+}, Sm^{3+}, Er^{3+}, and Y^{3+} at P1 increased (Figures 3c, S2b, S3b and S4b) and followed the order $Y^{3+} > Er^{3+} \approx Sm^{3+} > La^{3+}$.

To summarize, we find that factors, such as the water content, ion concentration in solution, and ion species, play important roles in the redistribution of voltage in the weathering crust soil. Generally, these factors contribute to the conductivity of the weathering crust soil in two ways, i.e., through solid-liquid interface and liquid phase conductivity. Differentiating between solution and solid-liquid interface conductivity can help optimize the leaching process of the EKM and monitor the migration paths of REE. For example, the REE concentration and water content can be predicted based on the conductivity of the weathering crust soil. Herein, it is vital to distinguish the conductivity of the solid-liquid interface and liquid phase, which is further studied in the following context.

3.2. Conductivity of the Dilute Solution and Original Weathering Crust Soil

To identify the conductivity of the liquid phase, a series of REE solutions with various concentrations were prepared. Figure 5a displayed the conductivity of La^{3+}, Sm^{3+}, Er^{3+}, and Y^{3+} solutions. It was found that the conductivities of all REEs increased linearly with increasing concentration. Furthermore, the conductivity was fitted by Equation (1) and the results are shown in Table 1. From Table 1, the conductivity and concentration show a high linear fit ($R^2 = 0.9977$ to 0.9993), and the conductivities of various REEs follow the order $Y^{3+} > La^{3+} > Sm^{3+} > Er^{3+}$. In infinite dilution, the equivalent ionic conductivities (λ) of these REEs follow the order of $La^{3+} > Sm^{3+} > Er^{3+} > Y^{3+}$. The highest conductivity of Y^{3+} results from the highest molar mass (138.91, 150.36, 167.26, and 88.91 g mol^{-1} for La, Sm, Er, and Y, respectively) of Y^{3+}.

Table 1. Parameters of the conductivity and diffusion coefficient of La^{3+}, Sm^{3+}, Er^{3+}, and Y^{3+} [43].

| Element	La^{3+}	Sm^{3+}	Er^{3+}	Y^{3+}
K	0.0899 ± 0.004	0.0747 ± 0.0011	0.0716 ± 0.0008	0.1262 ± 0017
R^2	0.9993	0.9977	0.9987	0.9980
λ (10^{-4} m^2 S mol^{-1}) [43]	69.7	68.5	65.9	62.0
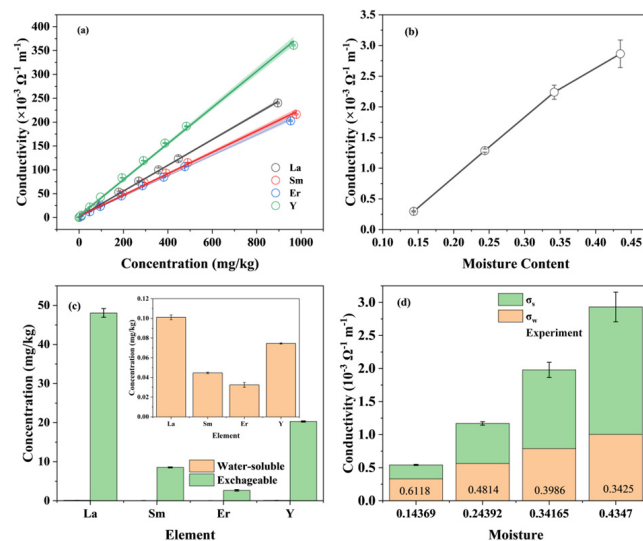
Figure 5. Conductivities of the La^{3+}, Sm^{3+}, $Er^{3+,}$ and Y^{3+} solution (**a**) and the weathering crust soil (**b**). The water-soluble and exchangeable concentrations of REE in the weathering-crust soil (**c**). The variations of σ_w and σ_s in different moisture contents in the weathering-crust soil (**d**).

Meanwhile, the conductivities of the original weathering crust soil were detected, and the results are shown in Figure 5b. From Figure 5b, it was found that the higher the moisture content, the larger the conductivity of the weathering crust soil. The conductivity of the original weathering crust soil (at the moisture content of 43.47%) reached 2.86×10^{-3} Ω^{-1} m^{-1}, which was close to previous studies [39,40].

In order to clarify the conductivity of the solid-liquid interface and liquid phase, the water-soluble and exchangeable concentrations of REE in the weathering crust soil were measured and results are shown in Figure 5c. In the weathering crust soil, the water-soluble concentration of REE was extremely low, which explains the low conductivity of the natural weathering crust soil. According to the water-soluble concentration of REE, the conductivity of liquid (σ_w) was calculated by Equation (1). The solid-liquid interface conductivity was calculated by the difference between the total and the liquid phase conductivities. The conductivity that resulted from the solid-liquid interface and liquid phase mechanism was distinctly shown in Figure 5d. It was found that the conductivity stemming from the pristine solution within the weathering crust soil was observed to diminish gradually as the moisture content increased, attributed to a reduction in ion concentration within the liquid phase. Consequently, the surface conductivity ratio escalated from 0.3882 to 0.6575, as depicted in Figure 5d, underscoring the significant contribution of the solid-liquid interface conductivity mechanism in the weathering crust soil.

3.3. Validation of the Extended Archie's Equation

To verify the feasibility of the extended Archie's equation, the effect of humidity, concentration, and species of REEs on the conductivity of the weathering crust soil were performed and the results were shown in Figure 6. It was found that the conductivity of the weathering crust soil increased by a factor of 5 with increasing the moisture content from 0.15 to ~0.45, despite the presence of La^{3+}, Sm^{3+}, Er^{3+}, or Y^{3+} with concentration of low, middle, or high. Similarly, the conductivity of the weathering crust soil increased by about 3~4 times when raising the REE concentration. In addition, the species of REE had an effect on the conductivity of the weathering crust soil due to the differences in ionic conductivity. Generally, the conductivity of REEs follows the order $Y^{3+} > La^{3+} > Sm^{3+} > Er^{3+}$ in similar concentration and humidity. For example, the conductivity of La-L, Sm-L, Er-L, and Y-L reached 7.50×10^{-3}, 7.28×10^{-3}, 6.56×10^{-3}, and 9.23×10^{-3} Ω^{-1} m^{-1}, respectively, at the moisture content of 0.39. The experimental results confirm that the conductivity of the weathering crust soil varies with the moisture content, REE concentration, and ionic species.
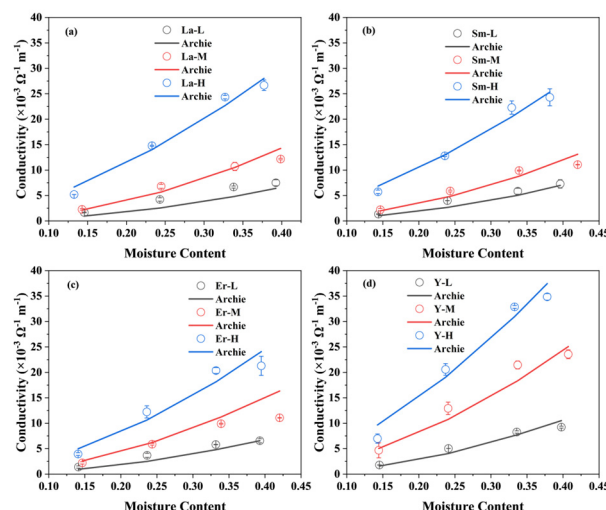
Figure 6. The experimental data and fitted curves by the extension of Archie's equation. The conductivity of the weathering crus soil in the presence of La^{3+} (**a**), Sm^{3+} (**b**), Er^{3+} (**c**), and Y^{3+} (**d**), at the low, middle, and high concentrations, respectively.

To quantify the conductivity of the solid-liquid interface and liquid phases, the water-soluble and exchangeable concentrations of the samples were investigated and the results were shown in Figure 7. As shown in Figure 7, the water-soluble (c_{aq}) and exchangeable REE concentrations (c_s) increased simultaneously. For example, the water-soluble concentration of La^{3+} increased from 1.84 to 93.14 mg L^{-1} with the increase of the exchangeable concentration of La^{3+} from 309.35 to 813.95 mg L^{-1}. Among these four REEs, the exchangeable concentration of Y^{3+} was lowest and the water-soluble concentration of Y^{3+} was highest in the weathering crust soil.
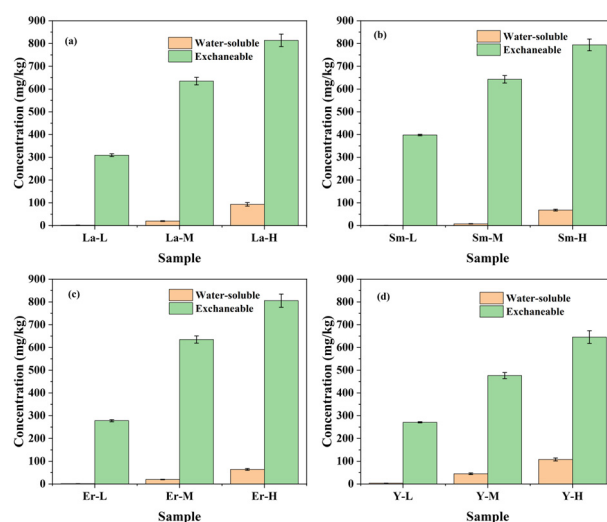
Figure 7. The water-soluble and exchangeable concentrations of La^{3+} (**a**), Sm^{3+} (**b**), Er^{3+} (**c**), and Y^{3+} (**d**) in the weathering crust soil.

When the water-soluble and exchangeable concentrations in the soil were determined, the conductivity of the weathering crust soil was verified by Equation (8). The fitting results are shown in Figure 6 and Table 2. As shown in Figure 6 and Table 2, all fittings were well with $R^2 > 0.9555$, which indicated that the extended Archie's equation was proper to describe the conductivity of the weathering crust soil. In addition, we identified that the parameters of K_1, K_2, and K_3 followed the order of $K_1 > K_2 > K_3$, suggesting that the soil humidity played the most important role in the conductivity.

Table 2. Parameters of conductivity for La^{3+}, Sm^{3+}, Er^{3+}, and Y^{3+}, respectively.

Parameters	Origin	La^{3+}	Sm^{3+}	Er^{3+}	Y^{3+}
K_1	71.2069 ± 59.6974	3.0512 ± 0.3148	4.9333 ± 0.4155	3.1722 ± 0.7320	2.4583 ± 0.3453
K_2	0.0428	0.0436	0.0363	0.0348	0.0613
K_3	0.0006 ± 0.0008	0.0127 ± 0.0022	0.0061 ± 0.0009	0.0120 ± 0.0039	0.0257 ± 0.0065
K_4	0.0100	0.0100	0.0100	0.0100	0.0100
R^2	0.9630	0.9708	0.9749	0.9555	0.9714

3.4. The Conductivity Mechanism of the Weathering Crust Soil

In IADs, the solid-liquid interface and liquid phase conductivity are two predominant conductivity mechanisms. As the extended Archie's equation can describe the conductivity of the weathering crust soil well, we applied it to calculate σ_w and σ_s in IADs in the presence of different concentrations of La^{3+}, Sm^{3+}, Er^{3+}, and Y^{3+} in order to distinguish the contribution of solid-liquid interface and liquid phase conductivity. The results are shown in Figure 8. The contribution of the solid-liquid interface and liquid phase conductivity is described by a K_{sw} ($K_{sw} = \frac{\sigma_s}{\sigma_w}$) value. At a low REE concentration, the K_{sw} was 16.58, 19.87, 28.80, and 13.26, for La^{3+}, Sm^{3+}, Er^{3+}, and Y^{3+}, respectively, suggesting that σ_s contributes more to the conductivity of the weathering crust soil. The contribution of σ_w is small due to excessive K_d ($K_d = \frac{c_s}{c_{aq}}$) (Figure 8). With increasing the REE concentration, the K_{sw} decreased, suggesting that the contribution of σ_s mechanism to the conductivity of the weathering crust soil fell because of the decrease in K_d. At a high REE concentration, σ_w even overtook σ_s as K_d was low, for example, the K_{sw} of La^{3+} was 0.83 at the La-H system.
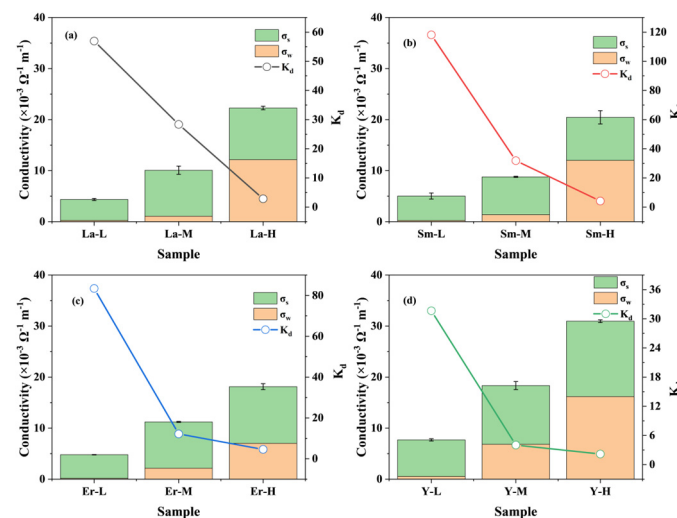
Figure 8. Comparison of the two conductivity mechanisms (solid-liquid interface and liquid conductivity mechanisms) to the conductivity of the weathering crust soil. The conductivity and K_d of the weathering crus soil in the presence of La^{3+} (**a**), Sm^{3+} (**b**), Er^{3+} (**c**), and Y^{3+} (**d**), respectively.

In the presence of different REEs (La^{3+}, Sm^{3+}, Er^{3+}, and Y^{3+}), the conductivity of the soil shows a discrepancy. On the one hand, the conductivities of La^{3+}, Sm^{3+}, Er^{3+}, and Y^{3+} in liquid were different (Figure 5). On the other hand, the adsorption capacities of various REEs on the soil were different (Figure 7). Both these factors lead to the diversity in the conductivities of the soil when adsorbing different REEs. At a low concentration, the contribution of K_{sw} to the soil conductivity followed the order of Er^{3+} > Sm^{3+} > La^{3+} > Y^{3+}. At a middle concentration, the value K_{sw} for La^{3+}, Sm^{3+}, Er^{3+}, and Y^{3+} decreased to 8.25, 5.36, 4.19, and 1.68 and followed the order of La^{3+} > Sm^{3+} > Er^{3+} > Y^{3+}. At a high concentration, K_{sw} for all REE decreases to approximately 1. Herein, the conductivity of the solid-liquid interface in the weathering crust soil cannot be ignored since it plays an important role in the conductivity of the weathering crust soil.

As revealed, the conductivity of weathering crust soil is mainly composed of solid-liquid interface and liquid phase conductivity mechanisms. However, the dominant conductivity mechanism will change with the REE concentration, soil humidity, and ion species. This is interesting and outstands the importance of distinguishing the soil conductivity mechanisms for a more precise description of the conductivity of the weathering crust soil. Moreover, a profound understanding of the soil conductivity mechanism guilds practical productions. For example, we can calculate the REE concentration and water content in the weathering soil during the EKM process by monitoring the conductivity of the soil.

3.5. Recalculating the Voltage in Weathering Crust Soil during EKM by the Extended Archie's Equation

By the extended Archie's equation, we can recalculate the voltage distribution in weathering crust soil during EKM. Another simulated EKM experiment with the injection of 400 ppm of REE solution in the anode were carried out, the results are shown in Figures S4–S7. For La^{3+}, Sm^{3+}, and Er^{3+}, the variations of voltages at P1–P4 were similar to that injected with 200 ppm of the solution. While for Y^{3+}, the voltage at P4 kept rising with increasing the EKM time, which may be attributed to that Y^{3+} and H^+ migrate too fast (Figure S8).

Initially, the electrical potentials of S1, S2, and S3 were calculated by the linear distribution model. As shown in Figure 9, the voltages of S1, S2, and S3 were 15.63 V if the voltage was linearly distributed in the column. However, experimental results suggest that the voltage of S1, S2, and S3 follow the order of S3 > S2 > S1. To characterize the deviation, the coefficient of determination (R^2) and mean squared error (E_{MSE}) are applied to correct the voltages of S1, S2, and S3.

$$R^2 = 1 - \frac{\sum_1^N (y_i - \hat{y}_i)^2}{\sum_1^N (\hat{y}_i - \overline{y_i})^2}, \ E_{MSE} = \frac{\sum_1^N (y_i - \hat{y}_i)^2}{N} \tag{9}$$

where N is the number of samples, y_i is the prediction from the numerical simulation by the extended Archie's equation or linear equation, $\hat{y}_i$ is the experimentally measured data, and $\overline{y}$ is the mean value of the experimentally measured data.
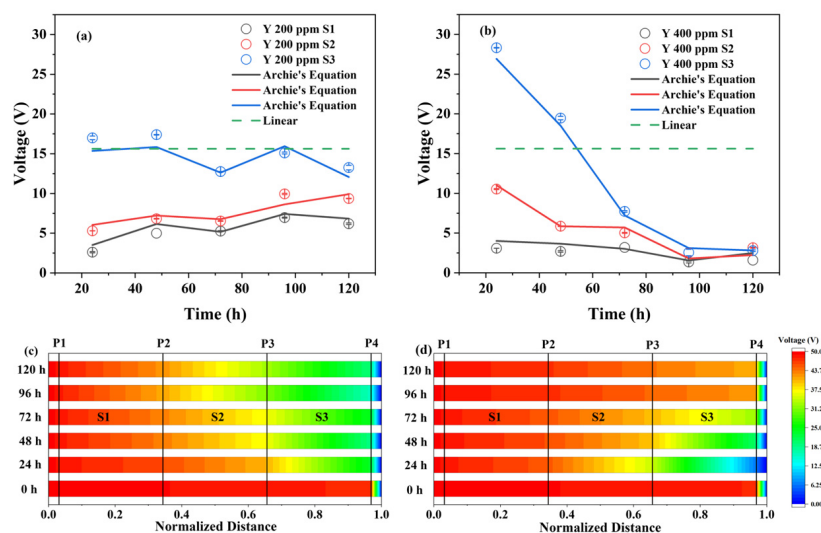
Figure 9. Variations of the soil voltages with increasing the EKM time at S1, S2, and S3 positions, respectively, as well as the simulated curves by Archie's equation and linear models with the injection of 200 (**a**) and 400 ppm (**b**) of Y^{3+} solutions. The variations in soil voltages were space interpolated in Origin 2023b with the injection of 200 (**c**) and 400 ppm (**d**) of Y^{3+} solutions.

The conventional linear model fitted the experimental data poorly based on the coefficient of determination and the mean squared error (Table 3). After calculating with the extended Archie's equation, the coefficient of determination and mean squared error

are improved as shown in Figure 9 and Table 3. Moreover, the fitting for Y^{3+} is better than that of La^{3+}, Sm^{3+}, and Er^{3+} (Figure S8). For Y^{3+}, there is no jump in voltage in S1, S2, and S3 after H^+ ions have migrated to P4 after 48 h as shown in Figure S4. However, for La^{3+}, Sm^{3+}, and Er^{3+}, the acidic front may have met the base front, resulting in a jump in voltage [21,44]. Herein, this acid-base reaction may have a great impact on the proposed model. Generally, the spatial and dynamical variations of the voltage in the weathering crust soil during EKM can be improved by the extended Archie's equation. Again, the model needs to be further refined to compensate for acid-base, ion exchange, precipitation reactions, and electrolysis.

Table 3. Parameters obtained from fittings of Archie's and linear models.

Model			La^{3+}	Sm^{3+}	Er^{3+}	Y^{3+}
Archie's	200 ppm	R^2	0.5518	0.5955	0.9195	0.9588
		E_{MSE}	77.6029	42.2672	13.0930	2.5608
	400 ppm	R^2	0.8764	0.5481	0.7512	0.9898
		E_{MSE}	13.2102	98.4102	28.0224	1.6515
Linear	200 ppm	R^2	−1.1453	−1.2282	−0.2263	−1.9304
		E_{MSE}	309.5636	194.0355	166.2313	151.6652
	400 ppm	R^2	−2.1521	−0.7130	−0.7731	−1.4903
		E_{MSE}	280.7236	310.8721	151.6652	335.1074

3.6. Predicting Water Content in Weathering Crust Soil during EKM by the Extended Archie's Equation

In nature, the water distribution in the soil is uneven. With the identical injection strategy used in the EKM process, some areas are supersaturated, while some areas are in the water shortage. This reduces the efficiency of EKM. Hence, obtaining water contents in distinct positions of the soil provides a strong basis for optimizing the addition of leaching agents. Various methods have been developed to measure the water content of soils in the field, such as seismic refraction [45], induced polarization [46], and nuclear geophysical [47] methods. Among these, measuring the soil conductivity by the four-electrode resistance method [48] to inverse moisture content of weathering crust soil by the extended Archie's equation is a convenient and economical way. Figure 10a displayed the conductivity of the weathering crust soil. It is observed that soil conductivities in various positions were all low, indicating that the moisture content and salinity of the weathering crust soil were low. The moisture contents of the weathering crust soil were calculated by the extended Archie's equation based on the measured conductivity. As shown in Figure 10b, the water contents were between 0.16–0.19, which is consistent with the measured data that the mean squared error was low and R^2 reached 0.8434. Based on the predicted moisture contents, we can optimize the leaching strategy during EKM. For example, if the initial moisture contents on the two sides are small, more leaching agent should be added; the area located at 6 m has the highest moisture content, so the amount of leaching agent should be reduced; the moisture contents in the rest areas were similar, the same amount of leaching agent should be added.
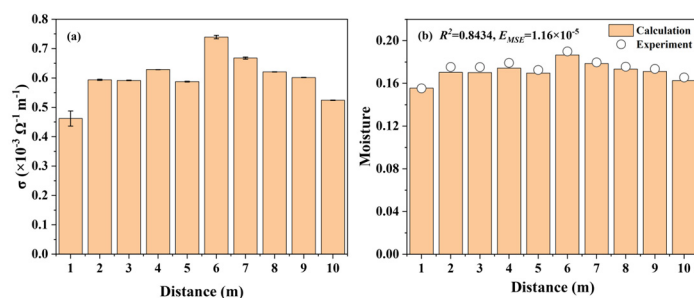
Figure 10. The conductivity (**a**) and moisture content (**b**) of the weathering soils in the field.

4. Conclusions

In summary, we have developed an extended Archie's equation for distinct REEs (i.e., La^{3+}, Sm^{3+}, Er^{3+}, and Y^{3+}, respectively) by incorporating conductivity mechanisms of both the solid-liquid interface and liquid phase via four-electrode resistance method. In dilute solution, the conductivity of REEs followed the linear model and the order $Y^{3+} > La^{3+} > Sm^{3+} > Er^{3+}$. In the weathering crust soil, the conductivity mechanisms change with increasing the moisture content and REE concentration, where the contribution of the liquid phase conductivity mechanism becomes large in a higher REE concentration. According to the R^2 and mean squared error, the calculated voltage of the weathering crust soil during EKM by using the extended Archie's equation is more reasonable than that by using the conventional linear model. Moreover, the extended Archie's equation is helpful to measure the water content (0.16–0.19) of the weathering crust soil in the field. However, the side effects including electrolysis, precipitation, and acid-base reaction affect the utilization of the model and the prediction becomes worse. In brief, this study adds new insights into the soil conductivity mechanism and provides a more reliable and convenient approach for monitoring the voltage distribution and water content of the weathering crust soil during EKM, which aids in designing EKM parameters, implementing the EKM process, and improving REE recovery. Moreover, the model needs to be further optimized in the future to suit more situations.

Conflicts of Interest: Authors declare that they have no competing interests.

Abbreviations

REEs: rare earth elements; HREEs, heavy rare earth elements; IADs, Ion-adsorption deposits; EKM, electrokinetic mining; LREEs, light rare earth elements; REE-L, the weathering crust soil soaked with 100 ppm of REE solution; REE-M, the weathering crust soil soaked with 300 ppm of REE solution; REE-H, the weathering crust soil soaked with 500 ppm of REE solution.

References

1. Chen, W.; Zhang, Z.; Long, F.; Chen, Z.; Chi, R. Rare Earth Occurrence States of Weathered Crust Elution-Deposited Rare Earth Ores in Southern Yunnan. *Minerals* **2023**, *13*, 554. [CrossRef]
2. Yang, X.J.; Lin, A.; Li, X.L.; Wu, Y.; Zhou, W.; Chen, Z. China's Ion-Adsorption Rare Earth Resources, Mining Consequences and Preservation. *Environ. Dev.* **2013**, *8*, 131–136. [CrossRef]
3. Hu, Q.; Yu, M.; Bi, D.; Liu, J.; Huang, M.; Zhu, A.; Song, Z.; Shi, X. Grain Size Analyses and Mineral Compositions of Core Sediments in the Western North Pacific Ocean: Implications for the Rare Earth Element and Yttrium Enrichment and Deposition Environment. *Minerals* **2023**, *13*, 1470. [CrossRef]
4. Xu, C.; Kynický, J.; Smith, M.P.; Kopriva, A.; Brtnický, M.; Urubek, T.; Yang, Y.; Zhao, Z.; He, C.; Song, W. Origin of Heavy Rare Earth Mineralization in South China. *Nat. Commun.* **2017**, *8*, 14598. [CrossRef]
5. Borst, A.M.; Smith, M.P.; Finch, A.A.; Estrade, G.; Villanova-de-Benavent, C.; Nason, P.; Marquis, E.; Horsburgh, N.J.; Goodenough, K.M.; Xu, C.; et al. Adsorption of Rare Earth Elements in Regolith-Hosted Clay Deposits. *Nat. Commun.* **2020**, *11*, 4386. [CrossRef]
6. Zeng, X.; Zeng, B.; Huang, L.; Zhong, L.; Li, X.; Huang, W. Adsorption of Y(III) on the Interface of Kaolinite-H$_2$O: A DFT Study. *Minerals* **2022**, *12*, 1128. [CrossRef]
7. Luo, X.; Zhang, Y.; Zhou, H.; He, K.; Luo, C.; Liu, Z.; Tang, X. Review on the Development and Utilization of Ionic Rare Earth Ore. *Minerals* **2022**, *12*, 554. [CrossRef]
8. Zhang, Z.; Zhou, C.; Chen, W.; Long, F.; Chen, Z.; Chi, R. Effect of Surfactant Addition on Leaching Process of Weathered Crust Elution-Deposited Rare Earth Ores with Magnesium Sulfate. *Metals* **2023**, *113*, 1112. [CrossRef]
9. Zhang, Q.; Ren, F.; Li, F.; Chen, G.; Yang, G.; Wang, J.; Du, K.; Liu, S.; Li, Z. Ammonia Nitrogen Sources and Pollution along Soil Profiles in an In-Situ Leaching Rare Earth Ore. *Environ. Pollut.* **2020**, *267*, 115449. [CrossRef]
10. Feng, J.; Yu, J.; Huang, S.; Wu, X.; Zhou, F.; Xiao, C.; Xu, Y.; Chi, R. Effect of Potassium Chloride on Leaching Process of Residual Ammonium from Weathered Crust Elution-Deposited Rare Earth Ore Tailings. *Miner. Eng.* **2021**, *163*, 106800. [CrossRef]
11. Tian, J.; Tang, X.; Yin, J.; Luo, X.; Rao, G.; Jiang, M. Process Optimization on Leaching of a Lean Weathered Crust Elution-Deposited Rare Earth Ores. *Int. J. Miner. Process.* **2013**, *119*, 83–88. [CrossRef]
12. Wang, G.; Xu, J.; Ran, L.; Zhu, R.; Ling, B.; Liang, X.; Kang, S.; Wang, Y.; Wei, J.; Ma, L.; et al. A Green and Efficient Technology to Recover Rare Earth Elements from Weathering Crusts. *Nat. Sustain.* **2023**, *6*, 81–92. [CrossRef]
13. Meng, X.; Zhao, H.; Zhao, Y.; Shen, L.; Gu, G.; Qiu, G. Heap Leaching of Ion Adsorption Rare Earth Ores and REEs Recovery from Leachate with Lixiviant Regeneration. *Sci. Total Environ.* **2023**, *898*, 165417. [CrossRef]
14. Yang, L.; Wang, D.; Li, C.; Sun, Y.; Zhou, X.; Li, Y. Searching for a High Efficiency and Environmental Benign Reagent to Leach Ion-Adsorption Rare Earths Based on the Zeta Potential of Clay Particles. *Green Chem.* **2018**, *20*, 4528–4536. [CrossRef]
15. Pires, C.M.G.; de Araújo Ponte, H.; Pereira, J.T.; de Santana Ponte, M.J.J. Yttrium Extraction from Soils by Electric Field Assisted Mining Applying the Evolutionary Operation Technique. *J. Clean. Prod.* **2019**, *227*, 272–279. [CrossRef]
16. Pires, C.M.G.; Pereira, J.T.; Ribeiro, A.B.; Ponte, H.A.; Ponte, M.J.J.S. Optimization of Electric Field Assisted Mining Process Applied to Rare Earths in Soils. *Appl. Sci.* **2021**, *11*, 6316. [CrossRef]
17. Pires, C.M.G.; Ribeiro, A.B.; Mateus, E.P.; Ponte, H.A.; Ponte, M.J.J.S. Extraction of Rare Earth Elements via Electric Field Assisted Mining Applying Deep Eutectic Solvents. *Sustain. Chem. Pharm.* **2022**, *26*, 100638. [CrossRef]
18. Martens, E.; Prommer, H.; Sprocati, R.; Sun, J.; Dai, X.; Crane, R.; Jamieson, J.; Tong, P.O.; Rolle, M.; Fourie, A. Toward a More Sustainable Mining Future with Electrokinetic in Situ Leaching. *Sci. Adv.* **2021**, *7*, eabf9971. [CrossRef]
19. Fu, Y.; Horton, R.; Ren, T.; Heitman, J.L. A General Form of Archie's Model for Estimating Bulk Soil Electrical Conductivity. *J. Hydrol.* **2021**, *597*, 126160. [CrossRef]
20. Hasan, M.F.; Abuel-Naga, H. Effect of Temperature and Water Salinity on Electrical Surface Conduction of Clay Particles. *Minerals* **2023**, *13*, 1110. [CrossRef]
21. Cai, J.; Wei, W.; Hu, X.; Wood, D.A. Electrical Conductivity Models in Saturated Porous Media: A Review. *Earth-Sci. Rev.* **2017**, *171*, 419–433. [CrossRef]
22. Park, S.S.; Hwang, M.J.; Moon, S.S.; Youn, H.Y. An Efficient VoD Scheme Providing Service Continuity for Mobile IPTV in Heterogeneous Networks. In Proceedings of the 2010 10th IEEE International Conference on Computer and Information Technology, 7th IEEE International Conference on Embedded Software and Systems (ICESS-2010), Bradford, UK, 29 June–1 July 2010; Volume 180, pp. 2589–2595.

23. Su, F.; Wu, J.; Wang, D.; Zhao, H.; Wang, Y.; He, X. Moisture Movement, Soil Salt Migration, and Nitrogen Transformation under Different Irrigation Conditions: Field Experimental Research. *Chemosphere* **2022**, *300*, 134569. [CrossRef]

24. Samouëlian, A.; Cousin, I.; Tabbagh, A.; Bruand, A.; Richard, G. Electrical Resistivity Survey in Soil Science: A Review. *Soil Tillage Res.* **2005**, *83*, 173–193. [CrossRef]

25. Brunner, G. Properties of Pure Water. In *Supercritical Fluid Science and Technology*; Elsevier: Amsterdam, The Netherlands, 2014; Volume 5, ISBN 9780444594136.

26. Kusim, A.S.; Abdullah, N.E.; Hashim, H.; Beeran Kutty, S. Effects of Salt Content on Measurement of Soil Resistivity. In Proceedings of the 2013 IEEE 7th International Power Engineering and Optimization Conference (PEOCO), Langkawi, Malaysia, 3–4 June 2013; pp. 124–128.

27. El Alam, J.; Revil, A.; Dick, P. Influence of the Water Content on the Complex Conductivity of Bentonite. *Eng. Geol.* **2023**, *322*, 107183.

28. Saarenketo, T. Electrical Properties of Water in Clay and Silty Soils. *J. Appl. Geophys.* **1998**, *40*, 73–88. [CrossRef]

29. Lee, S.S.; Fenter, P.; Nagy, K.L.; Sturchio, N.C. Real-Time Observation of Cation Exchange Kinetics and Dynamics at the Muscovite-Water Interface. *Nat. Commun.* **2017**, *8*, 15826. [CrossRef]

30. Ko, H.; Choo, H.; Ji, K. Effect of Temperature on Electrical Conductivity of Soils—Role of Surface Conduction. *Eng. Geol.* **2023**, *321*, 107147. [CrossRef]

31. Sikiru, S. Ionic Transport and Influence of Electromagnetic Field Interaction within Electric Double Layer in Reservoir Sandstone. *J. Mol. Liq.* **2021**, *344*, 117675. [CrossRef]

32. Keh, H.J.; Hsu, W.T. Electric Conductivity of a Suspension of Charge Colloidal Spheres with Thin but Polarized Double Layers. *Colloid. Polym. Sci.* **2002**, *280*, 922–928. [CrossRef]

33. Mojid, M.A.; Cho, H. Wetting Solution and Electrical Double Layer Contributions to Bulk Electrical Conductivity of Sand–Clay Mixtures. *Vadose Z. J.* **2008**, *7*, 972–980. [CrossRef]

34. Whittaker, M.L.; Comolli, L.R.; Gilbert, B.; Banfield, J.F. Layer Size Polydispersity in Hydrated Montmorillonite Creates Multiscale Porosity Networks. *Appl. Clay Sci.* **2020**, *190*, 105548. [CrossRef]

35. Xian, Z.; Hao, Y.; Zhao, Y.; Song, S. Quantitative Determination of Isomorphous Substitutions on Clay Mineral Surfaces through AFM Imaging: A Case of Mica. *Colloids Surfaces A Physicochem. Eng. Asp.* **2017**, *533*, 55–60. [CrossRef]

36. Naseri Boroujeni, S.; Liang, X.; Maribo-Mogensen, B.; Kontogeorgis, G.M. Comparison of Models for the Prediction of the Electrical Conductivity of Electrolyte Solutions. *Ind. Eng. Chem. Res.* **2022**, *61*, 3168–3185. [CrossRef]

37. Yang, M.; Liang, X.; Ma, L.; Huang, J.; He, H.; Zhu, J. Adsorption of REEs on Kaolinite and Halloysite: A Link to the REE Distribution on Clays in the Weathering Crust of Granite. *Chem. Geol.* **2019**, *525*, 210–217. [CrossRef]

38. Nouveau, M.; Grandjean, G.; Leroy, P.; Philippe, M.; Hedri, E.; Boukcim, H. Electrical and Thermal Behavior of Unsaturated Soils: Experimental Results. *J. Appl. Geophys.* **2016**, *128*, 115–122. [CrossRef]

39. Lide, D.R.; Baysinger, G. *CRC Handbook of Chemistry and Physics*; CRC Press: Boca Raton, FL, USA, 2005.

40. Corwin, D.L.; Scudiero, E. Field-Scale Apparent Soil Electrical Conductivity. *Soil Sci. Soc. Am. J.* **2020**, *84*, 1405–1441. [CrossRef]

41. Li, H.; Liu, X.; Hu, B.; Biswas, A.; Jiang, Q.; Liu, W.; Wang, N.; Peng, J. Field-Scale Characterization of Spatio-Temporal Variability of Soil Salinity in Three Dimensions. *Remote Sens.* **2020**, *12*, 4043. [CrossRef]

42. Olaojo, A.A.; Oladunjoye, M.A. Field-Scale Apparent Electrical Conductivity Mapping of Soil Properties in Precision Agriculture. *Rev. Bras. Geofis.* **2022**, *40*, 1–31. [CrossRef]

43. Archie, G.E. The Electrical Resistivity Log as an Aid in Determining Some Reservoir Characteristics. *Trans. AIME* **1942**, *146*, 54–62. [CrossRef]

44. Shah, S.A.; Shah, S.H.; Bibi, A.; Jadoon, Q.K.; Latif, K. Petrophysical Evaluation Using the Geometric Factor Theory and Comparison with Archie Model. *J. Nat. Gas Sci. Eng.* **2020**, *82*, 103465. [CrossRef]

45. Mctigue, D.; Horton, R.; Illman, W.A.; Helmke, M.F. Physical Properties of Rocks. *Dev. Pet. Sci.* **1982**, *12*, 147–253.

46. Martinho, E. *Electrical Resistivity and Induced Polarization Methods for Environmental Investigations: An Overview*; Springer International Publishing: Berlin/Heidelberg, Germany, 2023; Volume 234, ISBN 0123456789.

47. Zhang, F.; Zhang, C. Probing Water Partitioning in Unsaturated Weathered Rock Using Nuclear Magnetic Resonance. *Geophysics* **2021**, *86*, WB131–WB147. [CrossRef]

48. Rostami, H.; Osouli, A. *Electrical Resistivity Changes in Wet and Dry Side of Optimum Moisture Content for Soils with Low to High Fines Content BT—Advances in Transportation Geotechnics IV*; Tutumluer, E., Nazarian, S., Al-Qadi, I., Qamhia, I.I.A., Eds.; Springer International Publishing: Cham, Switzerland, 2022; ISBN 978-3-030-77234-5.